Model Reveals Joint Properties for Which Co-contracting Antagonist Muscles Increases Joint Stiffness

Isabella Kudyba and Nicholas S. Szczecinski(B)

West Virginia University, Morgantown, WV 26506, USA
nicholas.szczecinski@mail.wvu.edu

Abstract. A challenge in robotics is to control interactions with the environment by modulating the stiffness of a manipulator's joints. Smart servos are controlled with proportional feedback gain that is analogous to torsional stiffness of an animal's joint. In animals, antagonistic muscle groups can be temporarily coactivated to stiffen the joint to provide greater opposition to external forces. However, the joint properties for which coactivation increases the stiffness of the joint remain unknown. In this study, we explore possible mechanisms by building a mathematical model of the stick insect tibia actuated by two muscles, the extensor and flexor tibiae. Muscle geometry, passive properties, and active properties are extracted from the literature. Joint stiffness is calculated by tonically activating the antagonists, perturbing the joint from its equilibrium angle, and calculating the restoring moment generated by the muscles. No reflexes are modeled. We estimate how joint stiffness depends on parallel elastic element stiffness, the shape of the muscle activation curve, and properties of the force-length curve. We find that co-contracting antagonist muscles only stiffens the joint when the peak of the force-length curve occurs at a muscle length longer than that when the joint is at equilibrium and the muscle force versus activation curve is concave-up. We discuss how this information could be applied to the control of a smart servo actuator in a robot leg.

Keywords: Hill muscle · musculoskeletal modeling · insect · leg · joint · servo

1 Introduction

In biologically-inspired robotics, a limitation to function and mobility is the materials and devices available to construct and control robots. A common and readily-available actuator for robot limbs is the servo motor. The speed and position of a servo motor are easily controllable via feedback control, but the output torque must also be controlled if the robot is to interact with the environment and people properly (e.g., as in impedance control (Hogan 1985)). In nature, animals have evolved over millions of years to interact with their environment (e.g., walking, running, climbing) without damaging themselves or their environment and serve as a model for how robots may more readily control the forces they exert on the world. If the force control of animals can be mimicked by robots, then their motion may become less "robotic" and they may become more capable of walking and accomplishing other tasks.

F. Meder et al. (Eds.): Living Machines 2023, LNAI 14158, pp. 3–19, 2023.
https://doi.org/10.1007/978-3-031-39504-8_1

Animals may control the forces they exert on the environment by controlling the stiffness of their joints (Houk 1979). Animals have groups of antagonistic muscles that apply moments about the joints to move the body, e.g., the biceps and triceps muscles in the human arm that flex and extend the elbow joint. When simultaneously activated (i.e., "co-contracted") by the nervous system, the muscles increase the stiffness of the joint (i.e., the moment exerted in response to a change in angle) and can do so at many different angles (Zajac 1989; Blickhan et al. 2007). In this way, animals can resist external forces while producing the same motion (Matheson and Dürr 2003; Zakotnik et al. 2006). However, the properties a joint must possess to have the ability to increase joint stiffness by co-contracting antagonist muscles remain unknown. To investigate this question, we modeled a pair of antagonistic muscles that actuate an insect leg joint.

To ensure our model is physiologically plausible, we based our work on extensive characterization and modeling of the stick insect extensor tibiae muscle and the dynamics of the femur-tibia joint (Guschlbauer et al. 2007; Blümel et al. 2012a, b; von Twickel et al. 2019). The tibia is actuated by an antagonistic pair of muscles, the extensor and flexor tibiae. These are pinnate muscles with relatively simple geometry, e.g., their lengths are approximately sinusoidal functions of the femur-tibia angle (Guschlbauer et al. 2007; von Twickel et al. 2019). As in these previous studies, we modeled each muscle as a Hill-type muscle with an elastic element in parallel with the contractile element. The contractile element's force is a function of the muscle's activation and is limited by a force-length curve. Experiments show that the shape of the force-length curve depends on the activation of the muscle (Guschlbauer et al. 2007; Blümel et al. 2012a). All these features are present in our model. However, because we are primarily interested in understanding the stiffness of the joint (not its entire impedance), we omit the force-velocity curve from our model. In addition, because the activation dynamics of the flexor tibiae have not been characterized, the antagonist muscles in our model are both tuned like the extensor tibiae. Such a model prevents us from obscuring underlying principles of joint stiffness due to asymmetrical muscle parameters.

In this study, we investigate how muscle co-contraction may increase joint stiffness by constructing a mathematical model of an antagonistic pair of muscles that actuate an insect leg joint. Our overall approach is to set the activation of each muscle, calculate the joint's equilibrium angle, displace the joint from equilibrium, calculate the restoring moment generated by the muscle forces, and use this information to calculate the joint's stiffness. We calculated the dependence of this stiffness on four parameters:

1. the presence of the parallel elastic element,
2. the shape of the function that maps muscle activation to contractile element force (i.e., sigmoidal or linear),
3. the shape of the force-length curve (i.e., sine function as in Blümel et al. 2012a or polynomial as in Shadmehr and Arbib 1992), and

4. whether or not the peak of the force-length curve depended on muscle activation (Blümel et al. 2012a).

We find that for the parameters of the extensor tibiae muscle, co-contracting the muscles only stiffens the joint if:

- the peak of the force-length curve occurs at a muscle length *longer* than the muscle at joint equilibrium length **OR**
- if the function that maps muscle activation to contractile element force is concave-up.

In the discussion, we summarize our findings, discuss their relevance to the neural control of animal behavior, and propose how these findings could be applied to the control of walking robots.

2 Methods

2.1 Joint Model

The stiffness of a muscle joint, k $\frac{mN \cdot mm}{rad}$, can be calculated following Eq. 1, where τ is the joint torque (mN · mm) and ϑ is the joint angle (rad). The joint stiffness can be represented as the derivative of the torque with respect to the angle,

$$k = \frac{d\tau}{d\vartheta}. \tag{1}$$

The force in each muscle can be calculated, and then the moment arm lengths of each muscle are crossed with the corresponding forces to calculate the torque applied to the joint, as shown in Fig. 1 and Eq. 2. In Eq. 2, F_{extn} and F_{flex} are the extensor and flexor forces, and r_{extn}, r_{flex} are the respective maximum moment arm lengths,

$$\tau = F_{extn} r_{extn} \sin\vartheta - F_{flex} r_{flex} \sin\vartheta. \tag{2}$$

In this model, the length of the moment arms changes as the angle changes. This model neglects any pinnation angle of muscles, because this angle is so small in comparison with the orientation of the muscles and femur themselves (Blümel et al. 2012a). In addition to this simplification, we have assumed that the muscle resting lengths, resting moment arm lengths, and optimal force outputs are equal in the extensor and flexor. In future work these values can be changed based on parameters measured from the flexor tibiae or other muscles that actuate other joints.

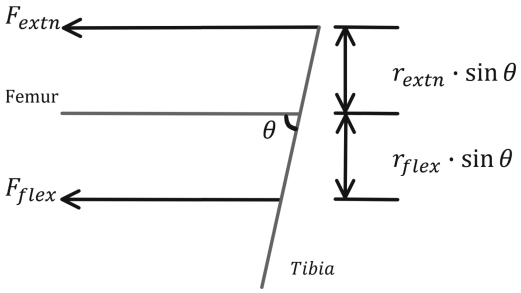

Fig. 1. Muscle forces produce a torque with moment arm lengths, r, that change with respect to the joint angle, ϑ.

2.2 Calculating Muscle Force

From the Hill-type muscle model, the force of a muscle is produced by a contractile element (CE), which is controlled by active dynamics from the nervous system, a parallel element (PE) that mimics the elastic and viscous forces of the inactivated muscle, and a series elastic element (SEE) that mimics the muscle's spring-like properties when activated (Zajac 1989). Because of their arrangement, the forces of the CE and PE add, and this sum is equal to the tension in the SEE, as well as the total force of the muscle. This relationship is shown in Eq. 3 and Fig. 2A,

$$F_{muscle} = F_{CE} + F_{PE} = F_{SEE}. \tag{3}$$

Note that previous studies by Blümel et al. (2012a) calculate muscle force as a function of the muscle fiber length, not muscle length (differentiated in Fig. 2B). However, we express our model in terms of muscle length, by replacing the fiber length with change of the muscle length, as a function of the joint angle and maximum moment arm lengths. As the joint angle increases, the length of the extensor decreases and the length of the flexor increases. The difference in these parameters does not impact the accuracy of this study but is noted for clarity.

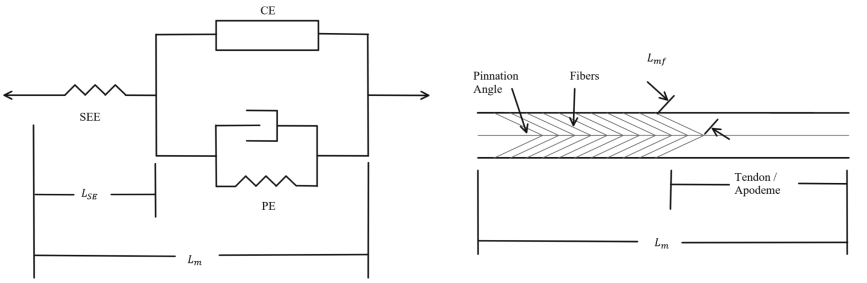

Fig. 2. A) The series elastic element (SEE), contractile element (CE), and parallel element (PE) produce the muscle force according to Eq. 4. B) The length of the muscle fibers compared to the length of the muscle.

The series elastic element produces a force shown in Eq. 4 where k_{SE} is the spring constant of the series elastic element and L_{SE} is the length of the series elastic element (Guschlbauer et al. 2007),

$$F_{SEE} = k_{SE} \cdot L_{SE}^2. \tag{4}$$

In steady state, the length of the muscle and force of the muscle do not change with time, so damping forces are omitted from the model. The elastic property of the parallel element follow Eq. 5, where k_1 and k_2 are spring constants and L_{mf} is the length of the muscle fibers (Blümel et al. 2012b). Figure 3 shows the relationship between F_{PE} and change in muscle length from the joint equilibrium length.

$$F_{PE} = k_1 e^{k_2 \cdot L_{mf}}. \tag{5}$$

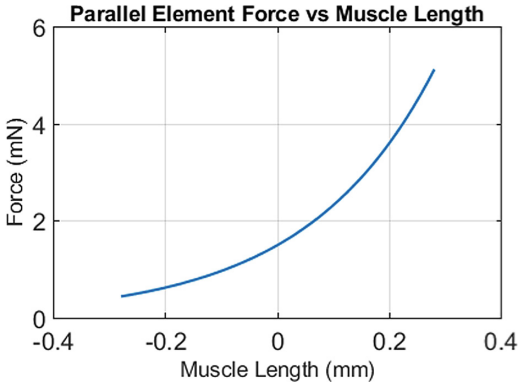

Fig. 3. Parallel element force against muscle length deviation from rest.

The contractile element (CE) produces force F_{CE} through activation dynamics, where excitation of the nervous system results in a force in the sarcomeres of the muscle tissue. F_{CE} depends on the maximum force that the muscle can produce, the activation of the muscle (A_{act}), the length of the muscle, and the speed at which the muscle is contracting (Zajac 1989). Because we are focusing on joint stiffness during tonic muscle activation, we are neglecting the speed at which the muscle is contracting. As a result, the contractile element force is the product of the maximum force the muscle can exert (F_{max}), the activation of the muscle, and a function of the muscle length (F_L) shown in Eq. 6 (Zajac 1989),

$$F_{CE} = F_{max} \cdot A_{act} \cdot F_L. \tag{6}$$

To account for the muscle activation component of the CE force, the normalized frequency of the motor neurons, f, is a fraction of maximum motor neuron excitation, normalized to 200 Hz, the maximum frequency observed in the extensor muscle during walking (Guschlbauer et al. 2007). In doing so this value can be thought of as a percentage of maximum excitation. Previous work shows that the motor neuron frequency does not

correlate linearly with the contractile element force, but instead is a sigmoid curve shown in Fig. 4 (Blümel et al. 2012a). When holding the extensor at the length which the joint is at equilibrium and exciting the extensor motor neuron, Blümel et al. measured the force output vs. motor neuron excitation. Note that in Blümel et al. 2012a, they refer to the normalized motor neuron frequency as *act*. They fit this curve, using Eqs. 7 and 8, where A_{act} represents the muscle activation. A_{act} is then used as a multiplier in Eq. 9 to calculate F_{CE} (Blümel et al. 2012a). Figure 4 shows the muscle force plotted against normalized motor neuron frequency, the rate at which the CE force increases with respect to this neuron excitation is larger at lower frequencies.

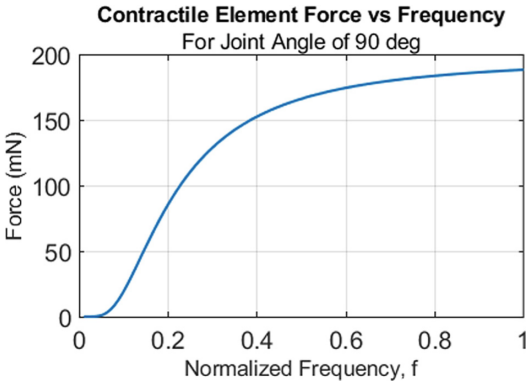

Fig. 4. Muscle force vs activation when the muscle is held at equilibrium angle. Accounted for in Eqs. 7 and 8.

Because of the actin/myosin filaments and cross bridges in the sarcomere, there is an optimized muscle length in which the contractile element can produce the greatest amount of force, and this happens when the muscle is stretched or is longer that at muscle length at joint equilibrium (Zajac 1989). Guschlbauer et al. found that at lower activation states, this peak occurs at a longer muscle length than at higher activations (Guschlbauer et al. 2007). Blümel et al. fit this phenomenon by describing the force-length relationship as a sine curve, which allowed for a shifting peak as muscle activation increased. This required the addition of a "frequency", ω (with units mm^{-1}), that is dependent on the motor neuron frequency. The calculation for ω is shown in Eq. 7, where $curv_\omega$ is an animal-dependent constant. Putting this all together, F_{CE} is shown in Eq. 9 and Fig. 5A (Blümel et al. 2012a),

$$\omega = 2.5 + \frac{1}{[curv_\omega \cdot (f + 0.05)]^2}, \tag{7}$$

$$A_{act} = 15e^{-1.06\omega}, \tag{8}$$

$$F_{CE} = F_{max} \cdot A_{act} \cdot F_L = F_{max} \cdot A_{act} \cdot \frac{1 + sin\omega L_{mf} - \frac{\pi}{2} + 2.7\omega}{2}. \tag{9}$$

Note that at very low activations, the equation produces a curve that does not follow the pattern at higher activations. This error is discussed further in the discussion.

To study the effects that each of these aspects has on the stiffness of the joint and create an estimate that can better be used in robotic applications, we analyze the CE force equation derived from Blümel et al. and create our own CE force equations that can be manipulated more easily in our model. Instead of a sine curve for the force-length curve, we use a parabola in vertex form, similar to the approach taken in other models (Cofer et al. 2010; Shadmehr and Arbib 1992). This allows us to shift the curve's peak easily, while maintaining similar force magnitudes from the constructed sine curve. To incorporate the non-linearity of the force and activation relationship, we can alter the muscles' activation, but we also test a linear relationship between the force and activation, when $A_{act} = f$. If a linear relationship produces a similar stiffness result to the non-linear relationship, the linear relationship may be used in servo-motor control to simplify and accelerate calculations. Equation 10 details the CE force we manipulate to compare with stiffness. In this equation, a changes the width of the curve, h shifts the peak with respect to the length of the muscle, and F_{max} is the maximum force of the curve,

$$F_{CE} = A_{act} \cdot a(L_m - h)^2 + F_{max}. \tag{10}$$

The shift in the force-length curve's peak can be altered with the activation state by using Eq. 11, where is machine epsilon. This was added so when the activation is 0, the result will not be undefined, but has a negligible effect on the shifting of the parabola. h_1 and h_2 are determined from the maximum and minimum peak shifts in the curve. These maximum and minimum shifts will resemble the look of the sine curve that was measured in the stick insect and can be shown in Fig. 5B. Note that $Shift_{max}$ was computed when normalized frequency is 10%. This adds little error to the equation at low frequencies:

$$h(f) = \frac{h_1}{f + } + h_2, \tag{11}$$

$$h_2 = \frac{Shift_{max} - 1}{1 - \frac{1}{Shift_{min}}}, \tag{12}$$

$$h_1 = Shift_{min} - h_2. \tag{13}$$

Figure 5 below compares the sine curve measured from the actual stick insect with the parabola function of Eq. 10 where the non-linear muscle activation is used, and the muscle length at which the peak of the parabola occurs decreases as activation increases. Figure 5C shows the parabola function where the length at which the peak occurs is constant and linear muscle activation relationship. Figure 5D shows the peak of the curve at a constant value, but with sigmodal activation. These different ways of calculating muscle force are labeled and detailed in Table 1 for further comparison.

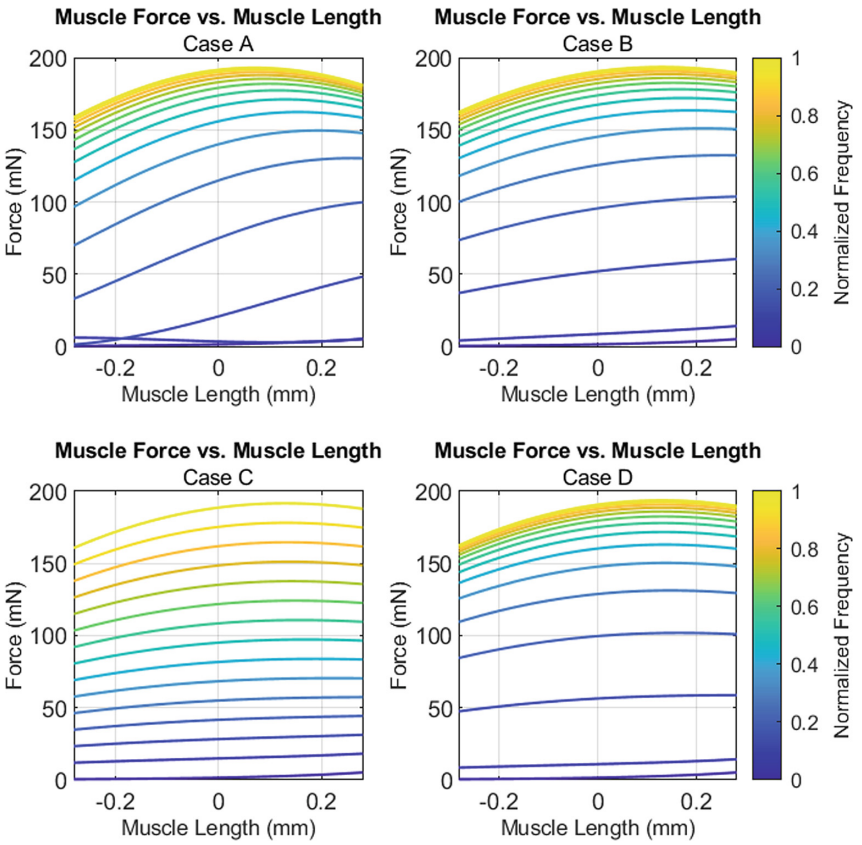

Fig. 5. A) Muscle force plotted against muscle length with increasing motor neuron frequency according to Blümel et al. (2012a). The equation for force is Case A detailed in Table 1. The force-length relationship is the sine curve measured from the actual stick insect. Note that at lower motor neuron frequencies, the equation produces maximum force at a very short length, which is addressed in the discussion. B) Muscle force using the parabolic force-length curve in vertex form, where h-shift in the peak of the graph is dependent on motor neuron frequency and muscle activation is non-linear. The force produced in this graph is Case B in Table 1. C) Muscle force using parabolic force-length curve, where h-shift in the peak of the graph is constant and muscle activation is linear. D) Muscle force using parabolic force-length curve, where h-shift is constant and muscle activation is nonlinear according to Eq. 8.

In Case C, the force-length relationship is modeled as a concave-down parabola. In this case, the parabola's shift along the length axis is not dependent on activation state, unlike in real muscles. Figure 6 compares the force-length curve for multiple levels of normalized frequency and values of h.

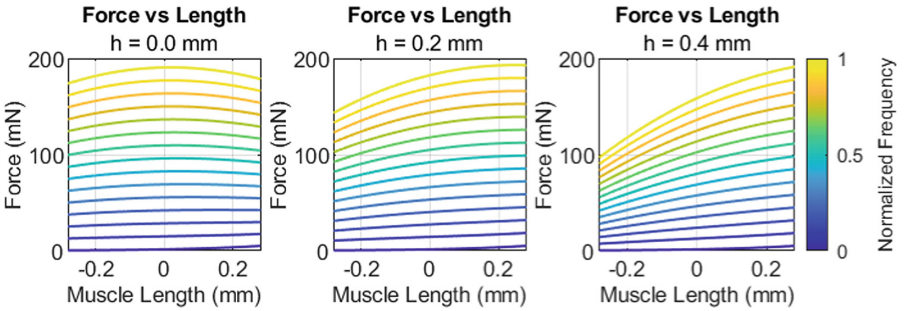

Fig. 6. Muscle force plotted against muscle length deviation from rest with increasing activation in Case C. Relationship plotted is the concave down parabola, where h represents a shift in the peak of the graph (i.e., the muscle length which produces the greatest active force).

2.3 Calculating the Stiffness

Using MATLAB R2022a, we calculate the force of each muscle by adding the contractile and passive forces for every angle and every activation state. The net torque is calculated and plotted for every activation combination of the extensor and flexor muscles. Figure 7 shows an example of torque vs. joint angle for equal coactivation. The stiffness was calculated using the centered difference approximation for the closest values of torque equal to zero, shown in Eq. 14. In this calculation, $\vartheta = 1^\circ = 0.017$ radian:

$$k = \frac{d\tau}{2\vartheta} \approx \frac{\tau(\vartheta + \vartheta) - \tau(\vartheta - \vartheta)\, d\vartheta}{}. \tag{14}$$

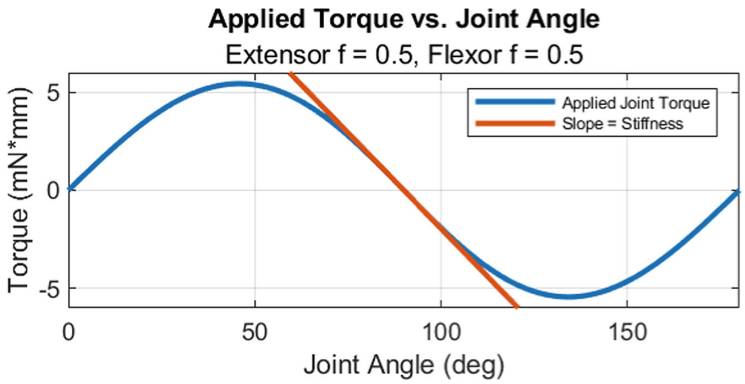

Fig. 7. Example Torque vs. Joint Angle plot used to calculate stiffness for set of activation combinations. Stiffness is calculated when torque is at the closest values to zero.

2.4 Testing Muscle Force Components

To analyze how different muscle parameters affect joint stiffness, we test different details that make up force, noted in Table 1. In the various cases, muscle force is calculated in

different ways. We compare Case A, the model derived in Blümel et al. (2012a) with Case B, sigmodal muscle activation according to Eq. 8, with the parabola force length curve, and a shifting peak of the curve according to Eq. 11. By comparing these cases we can demonstrate that the parabolic force-length curve produces a similar result to previous work measured in the stick insect joint.

To show how non-linear muscle activation affects joint stiffness, we compare Case C (linear muscle activation) to D (sigmodal muscle activation) with parabolic force-length curve and no activation-dependent peak shift. To show how shifting the peak of the

Table 1. Muscle Force Calculation Testing parameters

Case	Muscle Force Equation	Properties
A	$F_m = F_{max} \cdot A_{act} \cdot \frac{1 + \sin\left(\omega L_{mf} - \frac{\pi}{2} + 2.7\omega\right)}{2} + k_1 e^{k_2 \cdot L_{mf}}$	Muscle Activation: Sigmodal Force Length Curve: Blümel Sine Curve Force Length Peak: Dependent on f Parallel Element: Present
B	$F_m = A_{act} \cdot \left(a(L_m - h)^2 + F_{max}\right) + k_1 e^{k_2 \cdot L_{mf}}$, where $h = h(f)$ (Eq. 11)	Muscle Activation: Sigmodal Force Length Curve: Parabola Force Length Peak: Dependent on f Parallel Element: Present
C	$F_m = f \cdot \left[a(L_m - h)^2 + F_{max}\right] + k_1 e^{k_2 \cdot L_{mf}}$, where $h = \{0, 0.1, 0.2, 0.3, 0.4\}$	Muscle Activation: Linear Force Length Curve: Parabola Force Length Peak: Constant Parallel Element: Present
D	$F_m = A_{act} \cdot \left(a(L_m - h)^2 + F_{max}\right) + k_1 e^{k_2 \cdot L_{mf}}$, where $h = 0.1$	Muscle Activation: Sigmodal Force Length Curve: Parabola Force Length Peak: Constant Parallel Element: Present
E	$F_m = f \cdot \left(a(L_m - h)^2 + F_{max}\right) + k_1 e^{k_2 \cdot L_{mf}}$, where $h = h(f)$ (Eq. 11)	Muscle Activation: Linear Force Length Curve: Parabola Force Length Peak: Dependent on f Parallel Element: Present
F	$F_m = F_{max} \cdot A_{act} \cdot \frac{1 + \sin\left(\omega L_{mf} - \frac{\pi}{2} + 2.7\omega\right)}{2}$	Muscle Activation: Sigmodal Force Length Curve: Blümel Sine Curve Force Length Peak: Dependent on f Parallel Element: Absent
G	$F_m = A_{act} \cdot \left(a(L_m - h)^2 + F_{max}\right)$, where $h = h(f)$ Eq. 11)	Muscle Activation: Sigmodal Force Length Curve: Parabola Force Length Peak: Dependent on f Parallel Element: Absent

force-length curve affects joint stiffness, Case C includes multiple force-length curves with static but differing peaks between 0 mm and 0.4 mm.

Comparing Case C to E and Case D to B shows how the force-length curve's peak shifting dependence on motor frequency alters the stiffness, for a linear activation and the sigmodal activation, respectively. This analysis compares a constant peak shift to the peak shift dependent on motor neuron frequency according to Eq. 11.

Lastly, to analyze what affect the parallel element has on stiffness, in cases A and F we compare the Blümel et al. (2012a) model with and without the parallel element. Additionally, we compare the parabolic force-length curve with non-linear muscle activation and shifting peak with motor neuron frequency as observed in the animal, with and without the parallel element in Cases B and G.

The parameters used to calculate values of forces and their origin are listed in Table 2. Note that parameter values for the extensor muscle are used for both the extensor and flexor (see note in introduction). When choosing animal dependent parameters, animal E in Table 1 of Blümel et al. 2012b was used.

Table 2. Extensor parameter values used in model.

Parameter	Value	Source
r_{extn}	0.28 mm	Fig. 5 Guschlbauer et al. 2007
L_{mf}	1.41 mm	Fig. 3B Guschlbauer et al. 2007
F_{max}	189 mN	Table 1 Blümel et al. 2012b
$curv_{\omega}$	4.51 $mm^{0.5}$	Table 1 Blümel et al. 2012b
k_1	$3.13 \cdot 10^{-3}$ mN	Table 1 Blümel et al. 2012b
k_2	4.38 mm^{-1}	Table 1 Blümel et al. 2012b
a	$-200 \frac{mN}{mm_2}$	Not measured in animal
$Shift_{min}$	0.1 mm	Fig. 6a Blümel et al. 2012a
$Shift_{max}$	0.4 mm	Fig. 6a Blümel et al. 2012a

3 Results

Because the muscles in this model are equal and opposite, the equilibrium angle is 90 degrees when the muscles are activated the same amount. All stiffness graphs detailed below are plotted for a joint angle of 90 degrees. Figure 8 plots the joint stiffness against the motor neuron frequency for all cases listed in Table 1. Figure 8A shows Cases A through E and Fig. 8B shows Cases A, B, F, and G. Case A contains the most biological detail, including a sinusoidal force-length curve whose peak shifts to shorter lengths as muscle activation increases. Although the model contains some simplifications (see Methods), this model is likely closest to the animal's physiology. Co-activating the antagonist muscles increases the stiffness by a factor of 20 relative to the relaxed joint.

However, the joint stiffness decreases with muscle activation greater than approximation 20%. Furthermore, the stiffness of the joint is negative for some low motor neuron frequencies. This is due to the way the model from Blümel et al. (Eq. 9, Fig. 5A) maps from motor neuron frequency to muscle force. This is addressed in the Discussion.

Altering the form of the functions within the model shows the effect that each has on joint stiffness. When the sinusoidal force-length curve is replaced with a parabolic curve whose peak shifts with muscle activation (Case B), the peak stiffness is only about 8 times the baseline joint stiffness. Despite this difference, the maximum joint stiffness occurs at the same normalized frequency as in Case A, about 20%. This is where the inflection point of the activation curve occurs, suggesting that co-contracting antagonist muscles can stiffen the joint if the activation curve is concave-up. However, if the peak of the force-length curve does not shift with muscle activation (Case D), the joint stiffness always increases with increasing activation. This suggests that the location of the force-length curve's peak also affects joint stiffness. If the muscle activation is made a linear function of motor neuron frequency and the force-length parabola's peak is constant, the joint stiffness increases linearly with increasing motor neuron frequency (Case C). With linear activation and force-length curve peak shifting (Case E), stiffness increases linearly with motor neuron frequency and has a greater stiffness at lower frequencies.

Figure 8B enables the comparison of how the parallel element affects the stiffness of the joint. Because this element is in parallel with the contractile element, it simply raises the stiffness of the joint at all muscle activations.

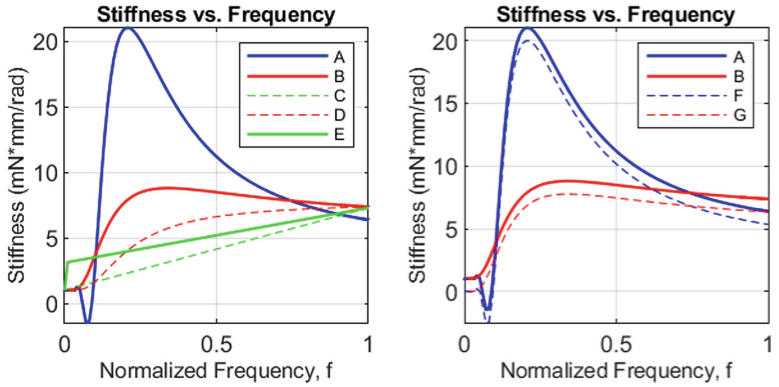

Fig. 8. A) Stiffness vs. Normalized motor neuron frequency for Cases A through E of Table 1. B) Stiffness vs. Normalized motor neuron frequency for Cases A, B, F, and G. Cases F and G are equivalent to Cases A and B respectively, minus the parallel element force.

Figure 9 shows the joint stiffness as a function of muscle activation for Case C in which the constant force-length curve peak shift is varied from 0 to 0.4 mm. As the peak of the force length curve is shifted a greater amount, the stiffness that the joint can achieve through co-contraction increases. When the peak shift is 0 mm, co-contracting the muscles does not stiffen the joint. This suggests that the force-length curve, a property of the active muscle, plays an important role in the stiffening of the joint during antagonist co-contraction.

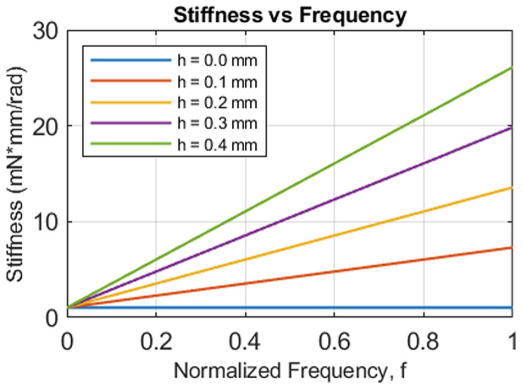

Fig. 9. Joint stiffness vs. muscle activation for Case C. Greater peak shifts (shown in Fig. 6) create greater maximum stiffness.

4 Discussion

To better understand how co-contracting antagonist muscles stiffens an animal's joint (Houk 1979; Blickhan et al. 2007), we developed a mathematical model of the muscular actuation of an insect joint based on experimental measurements and previous models (Guschlbauer et al. 2007, Blümel et al. 2012a, b; von Twickel et al. 2019). Each muscle in our model is a Hill muscle with a sigmoidal muscle activation curve, a parallel elastic element, a force-length curve, and an angle-dependent moment arm about the joint. Because we are interested in stiffness, we omitted the inertia of the distal limb segment and velocity-dependent terms in the muscle model, e.g., the force-velocity curve. By systematically altering the model, we found that co-activating the muscles increases joint stiffness if the peak of the force-length curve occurs at a muscle length longer than that at joint equilibrium or if the function that maps muscle activation to contractile element force is concave-up.

4.1 Limitations and Future Work

Although this study provided some insight into the joint properties by which co-contracting antagonist muscles may stiffen a joint, it has limitations as a model of the animal's joint. In the stick insect, the flexor muscle has a longer moment arm than the extensor, higher PE forces and maximum contractile forces, and unknown CE force-length dependence (Guschlbauer et al. 2007). Future studies may more accurately model the animal's joint by approximating the flexor's unique parameter values. To the authors' knowledge, no study measures the stiffness of the femoral/tibial joint in the stick insect and how it depends on muscle activation. Such data would be valuable for creating a more biologically accurate model.

Another limitation of this study is the omission of dynamic muscle properties, such as the force-velocity curve and the series elastic element. These properties are known to affect the force a muscle develops when the joint is disturbed from equilibrium (Zajac 1989; von Twickel et al. 2019). As a result, our model only approximates the full behavior

of a leg joint. Without these dynamic properties, our model most closely models a joint undergoing a slow perturbation, such that velocity-dependent effects do not dominate the response. In future work, we will incorporate these effects and test whether they affect joint stiffness during periods of co-contraction. We will also need a broader definition of stiffness than that in Eq. 1 that more broadly quantifies resistance to perturbations.

4.2 Implications of this Work

For the sine wave force-length curve proposed by Blümel et al. (Case A), the model deviates from the qualitative pattern at low motor neuron frequencies, with peak muscle force occurring at very short muscle lengths (Fig. 5A). This error occurs at 15% and less of normalized motor neuron frequency and is caused by a shifting in the sine curve. When data was taken from the stick insect, only muscle forces for some motor neuron frequencies were measured. When constructing the sine curve, Blümel et al. may not have accounted for motor neuron frequencies less than 30 Hz. Because of this, forces and stiffnesses measured with normalized frequencies less than 15% should be neglected when analyzing the sine curve data.

As an alternative to the sine force-length curve in Case A, we created the parabolic force-length curve in Case B (Fig. 5A and 5B). There are some differences in the magnitude of muscle force related to motor neuron frequency. At 10% of max normalized frequency, the largest percent difference between the two calculations for F_M for every joint angle was 106%, such a high value can be attributed to the error in the sine curve for frequencies less than 15% of maximum. However, at higher frequencies, the parabolic equation better matches the Blümel et al. sine curve. At 80% maximum normalized frequency, the largest percent difference between these two curves was 26%. At maximum motor neuron frequency, the largest percent difference was 6%. In future work, better approximations for the biological sine curve will allow for closer approximations for muscle force. When comparing the stiffness curves in Fig. 8A, Case A creates a noticeably greater joint stiffness than Case B, although the general shape of the curves is the same. Both curves produce a peak stiffness around 20% of maximum motor neuron frequency, and then decrease to a stiffness of about 7 $\frac{\text{mN}\cdot\text{mm}}{\text{rad}}$ at full motor neuron excitation. The difference in maximum stiffness is probably due to the non-linearity of the peak shifting noted in Eq. 11. We derived this equation as an approximation of the shifting of the peak in the sine curve, but its accuracy could be improved e.g., by replacing it with a second-order Taylor approximation of the sinusoidal relationship from Blümel et al. 2012a. However, because the shape of the stiffness curves in Fig. 8A is similar, we infer that the parabolic force-length curve does not fundamentally alter the behavior of the joint.

In Case C, when the peak of the force-length curve, h, is constant, shifting h to be longer increased the maximum stiffness the joint could produce, shown in Fig. 9. When the shift of the peak of the force length curve is zero, as in the F_{CE} is largest when the muscle is at joint equilibrium length, then the joint stiffness does not increase with increasing motor neuron frequency. For this reason, the maximum force that the muscle can provide must occur when the muscle is stretched past its length at joint equilibrium for stiffness to increase with motor neuron activation. The greater this shift, the greater stiffness the joint can produce. Comparing Case C (linear muscle activation and constant

peak shift) with Case D (sigmodal muscle activation and constant peak shift), we found that the non-linear muscle activation creates a non-linear relationship between motor neuron frequency and joint stiffness. The non-linear relationship between motor neuron frequency and muscle force also creates a maximum stiffness around 20% of maximum excitation.

When this peak shift is dependent on activation in Case E, $h = h(f)$, the dependency on motor neuron frequency in Case E increases the stiffness for lower frequencies, however the stiffness still increases with increasing frequency. This means that when the peak shift is a function of frequency, the maximum joint stiffness is not changed from the linear case when $h = 0.1$ mm, as shown in Case C in Fig. 8A.

Looking at Cases B and D allows us to compare how the stiffness changes with a peak dependent on motor neuron frequency when the muscle activation is nonlinear. Looking at Fig. 8A we observe that when the peak shift is dependent on motor neuron frequency (Case B) the maximum stiffness is much higher than in the constant peak case (Case D). Therefore, by comparing Cases C to E and Cases B to D we find that when the peak of the force length curve decreases with respect to motor neuron frequency, the stiffness that the joint can produce increases for lower motor neuron frequencies.

Lastly, we compare how removing the parallel element affects the stiffness in Cases A to F and B to G. When the parallel element was removed from the systems the magnitude of the stiffness decreases by a small amount and does not alter the relationship to motor neuron frequency, as shown in Fig. 8B. This phenomenon is observed both in the sine curve based (Case A) function and in the parabola function (Case B). Although including the parallel element in the model only increases the stiffness by little, the PE also sets the minimum stiffness the joint can have. If the PE were to be removed from the muscles, they would be allowed to have zero stiffness when activation is zero. To conclude, including the parallel element would be necessary for controlling a servo motor for setting minimum stiffness, but does not have much of an effect on stiffness at higher motor neuron firing frequencies.

4.3 Application to Robotics

Variable stiffness actuators (or more generally, variable impedance actuators) have been of interest in the field of robotics for several decades (for a review, see Wolf et al. 2016). Such actuators are of particular interest in the field of "collaborative robotics" (i.e., cobots), which must operate safely around humans (for a review, see Et Zaatari et al. 2019). Recently, some work has been done on modeling the joint stiffness of animals for use in robotics. Takuma et al. 2011 created a humanoid robot, *Kojiro*, with tendon-driven actuators that can resist applied forces from the environment by increasing the stiffness of joints. Zhang et al. 2022 analyzed the variable stiffness in human joints and neurological signals and matched them with a variable stiffness actuator to perform a lifting experiment. In both studies the actuators can change stiffness to adapt to the environment. However, the actuators in both cases were not just servo motors acting as a joint. For example, Kojiro's tendon-drive actuators are elastic bands that act as tendon and muscle, contracted by servo motors (Takuma et al. 2011). Zhang et al. 2022 implemented an extra stiffening motor with belt and circular springs surrounding the drive motor to stiffen the joint. These solutions are clever and effective, but add to the

size, weight, and mechanical complexity of the robot. In the future, we seek to apply the lessons learned from our current study to develop a software solution to be used with compact, commercially available smart-servo actuators. Nonetheless, more research is required to apply principles from animal muscle activation to develop more effective control strategies for the stiffness of a walking robot's leg joints in real time.

Acknowledgements. This work was funded by NSF DBI NeuroNex 2015317 to NSS. This work was also funded by NSF IIS 2113028 to NSS.

References

Blickhan, R., Seyfarth, A., Geyer, H., Grimmer, S., Wagner, H., Günther, M.: Intelligence by mechanics. Philos. Trans. R. Soc. A: Math. Phys. Eng. Sci. **365**(1850), 199–220 (2007). https://doi.org/10.1098/rsta.2006.1911

Blümel, M., Hooper, S.L., Guschlbauer, C., White, E.W., Büschges, A.: Determining all parameters necessary to build Hill-type muscle models from experiments on single muscles. Biol. Cybern. **106**(10), 543–558 (2012a). https://doi.org/10.1007/s00422-012-0530-5

Blümel, M., Guschlbauer, C., Daun-Gruhn, S., Hooper, S.L., Büschges, A.: Hill-type muscle model parameters determined from experiments on single muscles show large animal-to-animal variation. Biol. Cybern. **106**(10), 559–571 (2012b). https://doi.org/10.1007/s00422-012-0530-6

Cofer, D.W., Cymbalyuk, G., Reid, J., Zhu, Y., Heitler, W.J., Edwards, D.H.: AnimatLab: a 3D graphics environment for neuromechanical simulations. J. Neurosci. Methods **187**(2), 280–288 (2010). https://doi.org/10.1016/j.jneumeth.2010.01.005

El Zaatari, S., Marei, M., Li, W., Usman, Z.: Cobot programming for collaborative industrial tasks: an overview. Robot. Auton. Syst. **116**, 162–180 (2019). https://doi.org/10.1016/j.robot.2019.03.003

Guschlbauer, C., Scharstein, H., Buschges, A.: The extensor tibiae muscle of the stick insect: biomechanical properties of an insect walking leg muscle. J. Exp. Biol. **210**(6), 1092–1108 (2007). https://doi.org/10.1242/jeb.0272

Hogan, N.: Impedance control: an approach to manipulation: part I—theory. J. Dyn. Syst. Meas. Contr. **107**(1), 1–7 (1985). https://doi.org/10.1115/1.3140702

Houk, J.C.: Regulation of stiffness by skeletomotor reflexes. Annu. Rev. Physiol. **41**(1), 99–114 (1979). https://doi.org/10.1146/annurev.ph.41.030179.000531

Matheson, T., Dürr, V.: Load compensation in targeted limb movements of an insect. J. Exp. Biol. **206**(18), 3175–3186 (2003). https://doi.org/10.1242/jeb.00534

Shadmehr, R., Arbib, M.A.: A mathematical analysis of the force-stiffness characteristics of muscles in control of a single joint system. Biol. Cybern. **66**(6), 463–477 (1992). https://doi.org/10.1007/BF00204111

Takuma, S., Urata, J., Nakanishi, Y., Okada, K., Inaba, M.: Whole body adapting behavior with muscle level stiffness control of tendon-driven multijoint robot. In: IEEE International Conference on Robotics and Biomimetics (2011). https://doi.org/10.1109/robio.2011.6181623

Von Twickel, A., Guschlbauer, C., Hooper, S.L., Büschges, A.: Swing velocity profiles of small limbs can arise from transient passive torques of the antagonist muscle alone. Curr. Biol. **29**(1), 1-12.e7 (2019). https://doi.org/10.1016/j.cub.2018.11.016

Wolf, S., et al.: Variable stiffness actuators: review on design and components. IEEE/ASME Trans. Mechatron. **21**(5), 2418–2430 (2016). https://doi.org/10.1109/TMECH.2015.2501019

Zajac, F.E.: Muscle and tendon: properties, models, scaling, and application to biomechanics and motor control. Crit. Rev. Biomed. Eng. **17**(4), 359–411 (1989). https://doi.org/10.1113/jphysiol.1965.sp007626

Zakotnik, J., Matheson, T., Dürr, V.: Co-contraction and passive forces facilitate load compensation of aimed limb movements. J. Neurosci. **26**(19), 4995–5007 (2006). https://doi.org/10.1523/JNEUROSCI.0161-06.2006

Zhang, X., Huang, L., Niu, H.: Structural design and stiffness matching control of bionic variable stiffness joint for human-robot collaboration. Biomimetic Intell. Robot. **3**, 100084 (2022). https://doi.org/10.1016/j.birob.2022.100084